Materials Characterization 99 (2015) 210–219

Contents lists available at ScienceDirect

Materials Characterization

journal homepage: www.elsevier.com/locate/matchar

Magnesia tuned multi-walled carbon nanotubes–reinforced alumina nanocomposites

Iftikhar Ahmad [a,*], Mohammad Islam [a], Mushtaq Ahmad Dar [a], Fang Xu [b], Syed Ismat Shah [c], Yanqiu Zhu [d]

[a] Center of Excellence for Research in Engineering Materials, Advanced Manufacturing Institute, King Saud University, P.O. Box. 800, Riyadh 11421, Saudi Arabia
[b] Division of Materials, Mechanics and Structure, Faculty of Engineering, University of Nottingham, University Park, NG7 2RD, United Kingdom
[c] Department of Materials Science and Engineering, University of Delaware, Newark, DE 19716, USA
[d] College of Engineering, Mathematics and Physical Sciences, University of Exeter, Exeter EX4 4QF, United Kingdom

ARTICLE INFO

Article history:
Received 18 June 2014
Received in revised form 29 November 2014
Accepted 2 December 2014
Available online 3 December 2014

Keywords:
Nanocomposite
Carbon nanotube
Alumina
Microstructure
Mechanical properties
Magnesia

ABSTRACT

Magnesia tuned alumina ceramic nanocomposites, reinforced with multi-walled carbon nanotubes, were condensed using pressureless and hot-press sintering processes. Densification, microstructure and mechanical properties of the produced nanocomposites were meticulously investigated. Electron microscopy studies revealed the homogenous carbon nanotube dispersion within the alumina matrix and confirmed the retention of carbon nanotubes' distinctive tubular morphology and nanoscale features during the extreme mixing/sintering processes. Pressureless sintered nanocomposites showed meagre mechanical responses due to the poorly-integrated microstructures with a slight improvement upon magnesia addition. Conversely, both the magnesia addition and application of hot-press sintering technique resulted in the nanocomposite formation with near-theoretical densities (~99%), well-integrated microstructures and superior mechanical properties. Hot-press sintered nanocomposites incorporating 300 and 600 ppm magnesia exhibited an increase in hardness (10 and 11%), flexural strength (5 and 10%) and fracture toughness (15 and 20%) with respect to similar magnesia-free samples. Compared to monolithic alumina, a decent rise in fracture toughness (37%), flexural strength (22%) and hardness (20%) was observed in the hot-press sintered nanocomposites tuned with merely 600 ppm magnesia. Mechanically superior hot-press sintered magnesia tailored nanocomposites are attractive for several load-bearing structural applications.

1. Introduction

Carbon nanotubes (CNTs) have colossal interest due to their exceptional mechanical properties and functional traits thus being the front-runner reinforcing nanomaterial for contemporary ceramic composite technology [1,2]. Alumina (Al_2O_3) is an important structural ceramic material that is widely used in conventional industries and has promises for advanced load bearing structural applications like military armour system, aircraft engine parts and space engineering after curtailing its brittleness [3]. Therefore, a rigorous research work was conducted, over the last few years, to transfer the exceptional elasticity and strength of the CNTs to the brittle Al_2O_3 with numerous reports claiming success in this regard [4–10]. Although CNTs have refined the matrix grains and enhanced the strength, fracture toughness, wear resistance and electrical/thermal properties of the monolithic Al_2O_3 [11–13], the fabulous properties of CNTs could not be fully transferred to the nanocomposites due to hitches in obtaining even CNT distribution and near theoretical densities in the final nanocomposites, thus new strategies to address these challenges are in demand [4,5,14].

From literature, it seems that the mechanical properties of the CNT–reinforced Al_2O_3 nanocomposites could be further improved by tuning their microstructures using rare earth metal oxides [15,16]. In this perspective, microstructural modification of pure Al_2O_3 and Al_2O_3-based composites containing rare-earth metal oxides such as magnesia (MgO), cerium oxide (Ce_2O_3), lithia (Li_2O) and yttria (Y_2O_3) is an effective practice [17–20]. For example, small amounts (<1000 ppm) of Y_2O_3 doping into monolithic Al_2O_3 and ZrO_2–reinforced Al_2O_3 nanocomposites have shown notable improvements, resulting in high densities, defect-free microstructures and enhanced mechanical properties [19]. A recent study on the Y_2O_3 tuned Al_2O_3–CNT nanocomposites reported a higher (>99%) density, fivefold grain refinement and toughness enhancement of 40%, compared with the reference monolithic Al_2O_3 [20]. Similarly, small amounts of MgO (300 ppm) have been reported to reduce the effective sintering temperatures and restrict grain growth of Al_2O_3 reinforced with 5 vol.% silicon carbide (SiC) [21,22].

Besides these successes, the microstructural tweaking of the CNT–reinforced Al_2O_3 nanocomposites with MgO is rarely attempted. For this purpose, MgO-tuned Al_2O_3 ceramic nanocomposites reinforced with 2 wt.% multi-walled carbon nanotubes (MWCNTs) were fabricated

* Corresponding author at: Center of Excellence for Research in Engineering Materials (CEREM), Advanced Manufacturing Institute (AMI), King Saud University, P.O. Box: 800, Riyadh 11421, Saudi Arabia.
E-mail address: ifahmad@ksu.edu.sa (I. Ahmad).

http://dx.doi.org/10.1016/j.matchar.2014.12.002
1044-5803/

at elevated temperatures under pressureless (PL) and high-pressure (HP) sintering environments. The influence of small MgO additions (300 and 600 ppm) on the density, microstructure, grain size, hardness, flexural strength and fracture toughness of the nanocomposites is presented in this paper.

2. Materials and experimental procedures

2.1. Sample preparation

HP-sintering and PL-sintering techniques were used to fabricate Al_2O_3 matrix nanocomposites reinforced with 2 wt.% MWCNTs. Fig. 1 shows the fibre-like morphology and the multilayer tubular structures of the MWCNTs used as a reinforcing agent. MWCNTs were produced at Tsinghua University, Beijing, China with >90% purity and outer diameter, length and specific surface area values of ~40 nm, 0.8–2 μm and 60 m^2/g, respectively. The MWCNTs were chemically modified with H_2SO_4–HNO_3 solution and then dispersed into an aqueous solution containing small quantity (<1 wt.% of MWCNTs) of the surfactant sodium dodecyl sulphate (SDS, Sigma-Aldrich, United Kingdom) via sonication for 30 min using an ultrasonic probe (Sonic Processor D-100-20, Sonic system, United Kingdom). The aqueous MWCNT slurry was then incubated for 3 weeks, in order to obtain thorough adsorptions of the surfactant particles onto the MWCNT's surfaces. Nanopowders of γ-Al_2O_3 (ϕ30–40 nm, ≥98% pure specific surface area >40 m^2/g) and MgO (ϕ25–30 nm, 99.9% pure), obtained from Sigma-Aldrich, United Kingdom, were also incorporated at this stage according to the compositions given in Table 1. The suspension was re-sonicated for 120 min and divided into two equal batches after drying at 120–135 °C. One batch of the dried mixture was compacted into 12 mm diameter tablets at a pressure of 800 MPa using a high strength stainless steel mould and 50 ton Moore Hydraulic Press and subsequently sintered without external pressures at 1600 °C for 60 min under Ar atmosphere in a tube furnace (Elite, United Kingdom). The second batch of the mixture was separately hot-pressed (University of Mining and Technology, China) into ϕ32 mm diameter tablets under a constant pressure of 40 MPa at 1600 °C for 60 min under vacuum. In both sintering processes slow heating (10 °C/min) and cooling (30 °C/min) rates were maintained to prevent thermal spalling of the samples. Monolithic Al_2O_3 tablets were also fabricated using both sintering methods.

Table 1
Chemical compositions, densities and mechanical properties of the HP-sintered monolithic Al_2O_3 and nanocomposites with and without MgO tuning.

Matrix material	MgO contents (ppm)	CNT contents (wt.%)	Measured density g/cm^3	Flexural strength (σy)	Fracture toughness (K_{IC})	Modulus of elasticity (E)
				MPa	MPa·$m^{1/2}$	GPa
Al_2O_3	–	–	3.88 ± 0.01	340 ± 21	3.2 ± 0.1	392 ± 10
Al_2O_3	300	–	3.90 ± 0.02	346 ± 18	3.1 ± 0.2	388 ± 15
Al_2O_3	600	–	3.92 ± 0.01	355 ± 26	3.2 ± 0.1	390 ± 13
Al_2O_3	–	2	3.82 ± 0.02	390 ± 10	4.1 ± 0.3	370 ± 14
Al_2O_3	300	2	3.93 ± 0.01	410 ± 22	4.8 ± 0.2	364 ± 16
Al_2O_3	600	2	3.95 ± 0.01	435 ± 10	5.1 ± 0.3	353 ± 21

2.2. Density measurement and structural characterisation

Density of each sintered sample was measured by Archimedes method in distilled water, and the relative density was calculated by dividing apparent density with theoretical density. The theoretical density values for Al_2O_3, MgO and MWCNT were considered to be 3.97, 3.58 and 1.80 g/cm^3, respectively [22,23]. Structural features of the gold coated fractured samples were assessed using a scanning electron microscope (SEM, Philips/FEI-XL30). A Siemens D500 X-ray diffractometer with CuK_α radiation (DIFFRAC^{plus}, Bruker Advanced X-ray Solutions, Germany) was operated with 0.025°/s step size to (i) identify the crystalline phases and (ii) estimate the crystallite sizes of the sintered samples. Furthermore, the crystallite size was calculated by measuring the peak width (full-width-at-half-maximum, FWHM) in an X-ray diffraction pattern of the sintered polished samples, as given by Scherrer Eq. (1) [24],

$$t = \frac{K\lambda}{B\cos\theta} \tag{1}$$

where B is the FWHM value of a specific plane (hkl) in radians, λ is the wavelength of the incident X-rays, θ the centre angle of the peak, t the crystallite size and K is the crystallite shape factor, having a typical value of ~0.9. Thermal etching of all fine-polished samples was carried out at 1400 °C for 15 min under Ar atmosphere. Chemical etching method was practiced to prepare samples for transmission electron microscope

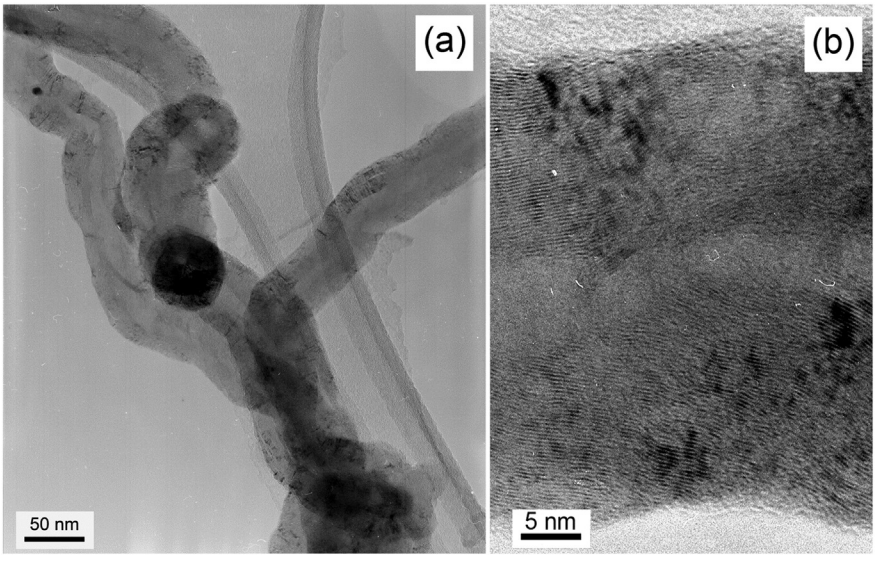

Fig. 1. TEM images of the pristine MWCNTs, (a) at low magnification, show fibrous morphology and nanoscale dimensions and (b) at high-resolution, demonstrate a multi-layered tubular structure.

(TEM) investigations. For this purpose, finely milled (<150 μm) HP-sintered nanocomposite samples were dipped into a NaOH solution for 2 weeks and then rinsed with distilled water several times to remove any NaOH traces. The cleaned samples so obtained were then suspended in acetone medium using ultra-sonication followed by transfer onto a holey carbon copper grid for further observation under TEM (JEOL 2000 FX, Japan) [12].

2.3. Mechanical testing

After fine polishing using 1 μm diamond suspension, microhardness testing of the resin bonded sintered samples was carried out at 9.8 N loads for 15 s by employing hardness tester (M-400, LECO, Japan). Pulse-echo reflectometry, a non-destructive ultrasonic technique, provides a simple method to estimate modulus of elasticity of the sintered samples. Compression measurements were made using a 20 MHz centre frequency using ϕ6 mm contact transducers (TMP-3) provided by Sonatest, UK. The equivalent shear measurements were performed with a 10 MHz centre frequency using a ϕ10 mm contact transducer (V221-BA) supplied by Panametrics, USA. Appropriate couplant materials such as oil and set honey were used in each case to ensure optimum contact between the samples and the transducers. From velocity measurements, the modulus of elasticity of the samples was calculated by employing Eq. (2) [14],

$$E = \frac{V_s^2 \rho \left(3V_c^2 - 4V_s^2\right)}{V_c^2 - V_s^2} \tag{2}$$

where E, ρ, V_c and V_s are Young's modulus, bulk density of the sample, compression velocity and shear velocity, respectively.

Flexural strength (σ_f) is defined as strength of a material during bending at the instant of failure and is expressed by the following equation (Eq. (3)) for a three-point bending test configuration [12],

$$\sigma_f = \frac{3FL}{2bd^2} \tag{3}$$

where F is the load at the fracture point, L is the span length, b the sample breath and d the sample thickness. In this study, the σ_f was measured by a three-point bending method using an INSTRON-5569 universal testing machine according to ASTM 1161-02c protocol. The breaking load was measured using a 5 kN load cell. For each test, three samples were cut from a hot-pressed disc using a resin-bonded diamond impregnated wafering blade (Buehler, Germany). The specimen dimensions were 25 ± 1.5 mm (l) × 3 ± 0.2 mm (b) × 2.5 ± 0.2 mm (d). Before testing, all faces of the sample were carefully polished to 1 μm roughness using a diamond paste. The bending span and the load speed were 20 mm and 0.5 mm/min, respectively.

In the direct crack measurement (DCM) method, the lengths of crack emerging from the corner of an indent generated during Vickers hardness tests are used to determine fracture toughness (K_{IC}). The crack lengths were carefully measured using SEM, within 1–2 h after indentation, and the recorded images were analysed utilising image processing and analysis software (ImageJ). The K_{IC} values were computed using Eq. (4) [11],

$$K_{IC} = 0.016\left(\frac{E}{H}\right)^{1/2}\left(\frac{P}{C^{3/2}}\right) \tag{4}$$

where E, H and C are the respective values of modulus of elasticity, microhardness (HV) and radial crack length generated through Vickers indentation.

3. Results and discussion

3.1. Dispersion and stability of MWCNTs

A homogenous dispersion of the MWCNTs within the base Al_2O_3 matrix is imperative to fabricate mechanically strong nanocomposites. Studies on the MWCNT–reinforced ceramics described that an adequate dispersion is attainable for up to 2 wt.% MWCNT reinforcement with further additions always resulting in poor quality nanocomposites, due to severe MWCNT agglomeration [12,16,20]. Keeping this in view, a wet chemistry route was adopted to disperse MWCNTs homogenously into the Al_2O_3 matrix as described elsewhere [14]. In short, high frequency ultrasonication, surfactant (SDS) and three week storage period for thorough attachment of surfactant (SDS) particles onto the MWCNT surfaces, all efficiently contributed to obtain even distribution of the MWCNTs within the parent Al_2O_3 matrix. SEM fractography (Fig. 2a and b) of the nanocomposite samples confirmed the even dispersion of the MWCNTs (marked with white arrows). The homogenous dispersion is believed to occur due to attachment of the hydrophobic MWCNTs to the hydrophobic tails of the SDS surfactant particles,

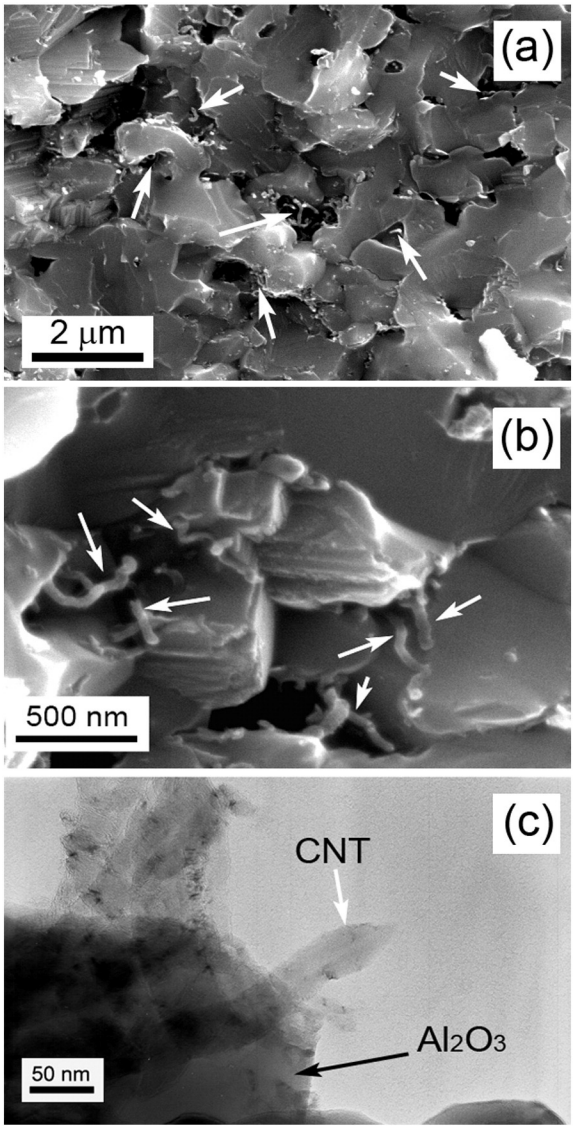

Fig. 2. SEM fractured surface images of the MgO tuned nanocomposites showing well-dispersed MWCNTs (white arrows) within Al_2O_3 grains at (a) low and (b) high magnifications and (c) TEM image of a MWCNT (white arrow) retrieved from sintered nanocomposites exhibiting its structural and morphological stability.

resulting in MWCNT surfaces being covered by positively-charged surfactant molecules. Such envelope increases the magnitude of steric hindrance between MWCNTs and counteracts the van der Waals interaction amongst them. Moreover, the sulfonic group in the surfactant (SDS), through adsorption onto the MWCNT surfaces, changes the wetting properties and makes MWCNTs hydrophilic, thus facilitating their dispersion in the matrix [16]. Besides showing success in the MWCNT distribution, Fig. 2 also provides interesting details concerning the physical and the structural stability of the MWCNTs, which negate doubts about their degradation during processes involving higher temperature and/or pressures [25,26]. High magnification SEM micrograph details obtained from analysis of the nanocomposite fractured surfaces (Fig. 2a and b) clearly show the typical fibrous-like tubular morphology with curly features, which depict the retention of the promising high elastic strain traits, predicted for the MWCNTs [2]. Furthermore, Fig. 2c shows the TEM microstructure of a chemically etched nanocomposite sample where a firm attachment of a tube-like structure of the MWCNT (white arrow) with the Al_2O_3 matrix (black arrow) is clearly visible. Such observations made during electron microscope studies corroborate with the idea that the MWCNTs are both mechanically and thermally stable, maintaining their tubular morphology and nanoscale features even under elevated temperatures and high pressure sintering environments. These findings, therefore, are well in-line with the inferences drawn from molecular dynamics simulation study for estimating physical, mechanical, structural and thermal stability of the MWCNTs [26].

3.2. Densification and structural features

Our results (Fig. 3a) show that with just 300 ppm and 600 ppm MgO additions the relative density of the PL-consolidated unreinforced Al_2O_3 was raised to 92% and 94%, respectively, which are 2 and 4% higher than that of PL-sintered pure Al_2O_3 (90%). In this context, studies explain that MgO efficiently controls the abnormal grain growth, pore mobility and O_2 loss from Al_2O_3 during the PL-sintering by altering the grain boundary chemistry, lattice structure and surface diffusivities, thereby leading it to higher density and fine microstructures [17,18,21,27].

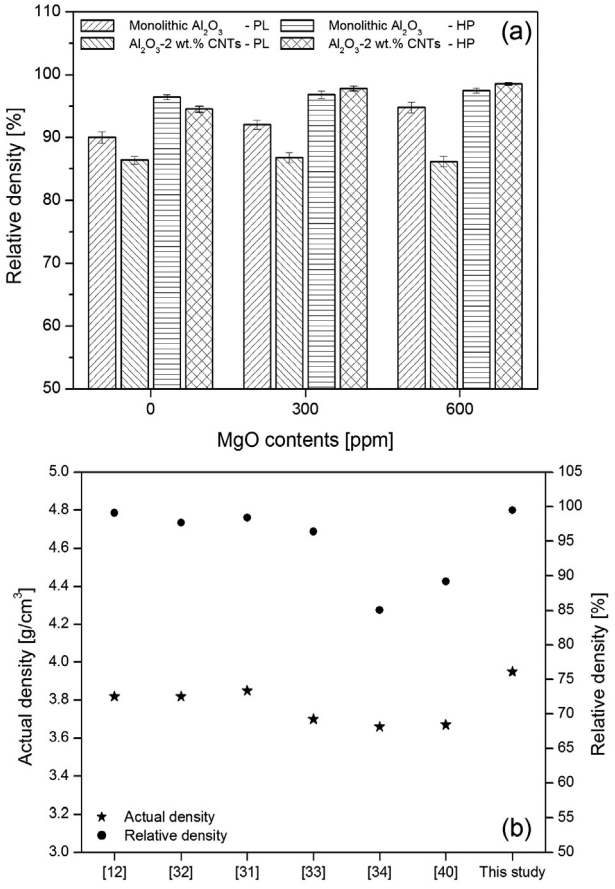

Fig. 3. (a) Densities of the monolithic Al_2O_3 and nanocomposite samples as the function of MgO concentrations, sintered under pressures and pressure-free conditions and (b) comparison of the density of MgO-doped nanocomposites with previous reports.

A relative density of 86% could be achieved after PL-sintering the nanocomposites, even with MgO doping at both levels, this barely contributed towards any density improvement (Fig. 3a). It is well-known that owing to the tubular morphology, high aspect ratio and thermal/chemical stability of the MWCNTs, material migration during the densification is restricted, thus preventing Al_2O_3 grain integration and adversely affecting the densification of nanocomposites upon sintering under pressure-free condition. Low magnification SEM fractographs of the PL-sintered nanocomposites revealed a heterogeneous microstructure containing isolated dense patches separated by microcracks (white arrows in Fig. 4b); whereas no such microstructural irregularities were observed in monolithic Al_2O_3 samples (Fig. 4a). MWCNTs seem to be the potential source of scanty densification of PL-sintered nanocomposites. The presence of heterogeneous microstructures maybe attributed to two potential reasons: (i) gaseous products (Al_2O and CO) are produced during the carbothermal reduction of Al_2O_3 by MWCNTs at elevated temperatures (~1600 °C) and it is quite possible that these gases gradually generated pressure inside the nanocomposite, producing microcracks as a consequence whilst escaping during subsequent cooling, and (ii) MWCNTs being an effective grain refinement agent hindered the Al_2O_3 grain growth during PL-sintering through segregating at grain boundaries in addition to restricting the grain coalescences, thus giving rise to porous or heterogeneous microstructures of the nanocomposites [16,28].

Conversely, the constant external pressures during HP-sintering consolidated both pure Al_2O_3 (Fig. 4c) and nanocomposite (Fig. 4d) into a well-integrated, dense and homogenous microstructure, without the above microstructural flaws, with high relative densities of 96.4 and 94.5%, which are 6 and 9% higher than their respective PL-sintered counterparts (Fig. 3a). It is most likely that high pressure prevalent during sintering simultaneously eliminated shrinkage-induced microcracks or the microcrack/void formation due to escape of gases generated during sintering, thus consequently consolidating the nanocomposites to higher densities by overcoming the hurdles arising from MWCNTs. Furthermore, Fig. 3a shows that the MgO doping of 300 or 600 ppm into nanocomposites of the same composition also raised the relative densities of the HP-sintered samples to 97.8 and 99.6%, an increment of 3 and 5%, compared with their MgO-free nanocomposite counterparts. These density increases suggest that MgO doping may have altered the sintering characteristics of Al_2O_3 in the nanocomposites during HP-sintering. Diminution of O_2 from Al_2O_3 during high temperature sintering (>1600 °C) is a known phenomenon that restrains Al_2O_3 matrix composites from attaining near-theoretical densities [29]. However, dopants like MgO influence the mass transport of the Al_2O_3 matrix grains by controlling the diffusion of Al^{3+} and O^{2-} ions as well as improve the thermal stability of Al_2O_3, thus resulting in nanocomposites with higher densities [30]. The significance of MgO doping in nanocomposites is also evident from graphical comparison (Fig. 3b) of the density results with earlier reports. For example Ahmad et al. [12], and Wie et al. [31], could obtain respective density values of 3.82 and 3.85 g/cm^3 for nanocomposites after HP-sintering, whereas Yamamoto et al. [32], sintered nanocomposites to a density of 3.82 g/cm^3 using SPS. Similarly, Ghobadi et al. [33], Ueda et al. [34], and Bakhsh et al. [36], reported low densities of 3.70, 3.66 and 3.67 g/cm^3, respectively, for PL-sintered nanocomposites with the same constituents. Our HP-sintered nanocomposites doped with 600 ppm MgO demonstrated a density of 3.95 g/cm^3, which is close to the theoretical density (99.6%). These details corroborate the combined importance of the external pressures and MgO, as dopant, during elevated temperature sintering

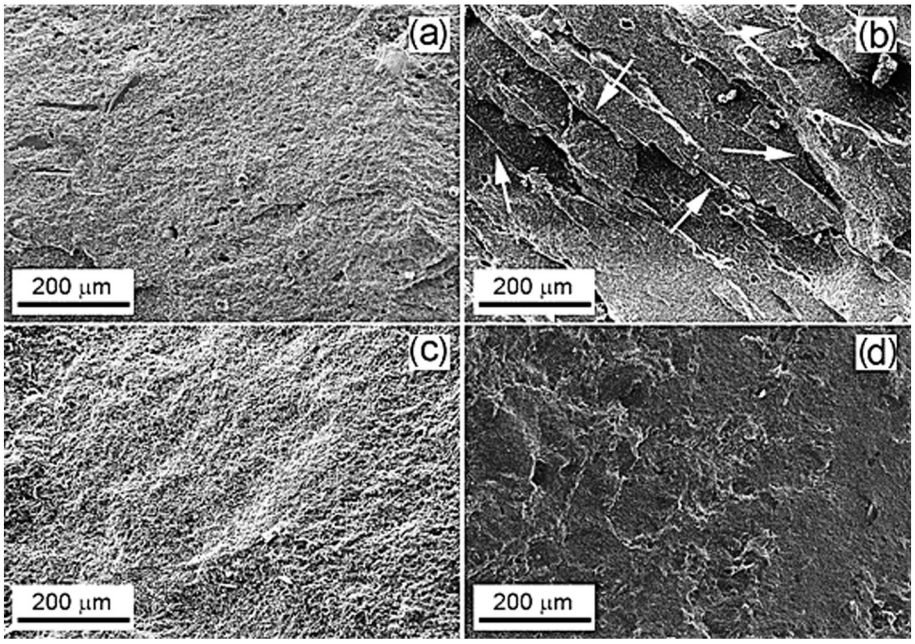

Fig. 4. Low magnification images of the SEM fractured surface details of the samples sintered without external pressures, 600 ppm MgO-doped (a) monolithic Al_2O_3, (b) nanocomposite, microcracks clearly visible (white arrows) and HP-sintered MgO-free (c) monolithic Al_2O_3, and (d) nanocomposite, exhibiting well-integrated flaw-free homogenous microstructure.

regimes in order to obtain advanced structures and properties in the MWCNT–reinforced Al_2O_3 nanocomposites.

3.3. Grain size analysis and fractography

Compared with the PL-sintered monolithic Al_2O_3, the grain sizes reduced by 11 and 19%, respectively, upon tuning with 300 and 600 ppm MgO, as evident from Fig. 5. Fig. 6a reveals the uneven grain growth in the undoped Al_2O_3, however, the MgO addition helped in the formation of finer and more uniform grains (Fig. 6b and c). Indeed, MWCNTs acted as a grain refining agent during the PL-sintering of the nanocomposites (Fig. 6d), and the surface microstructure of the MgO-free CNT/Al_2O_3 nanocomposite exhibits a 70% finer grain morphology than pure Al_2O_3. A further drop in the grain size by 5 and 28% was observed in the case of the PL-sintered nanocomposites tuned with 300 and 600 ppm MgO, respectively, as shown in Fig. 6e and f. In this context, it may be assumed that the MWCNTs are not present at all of the

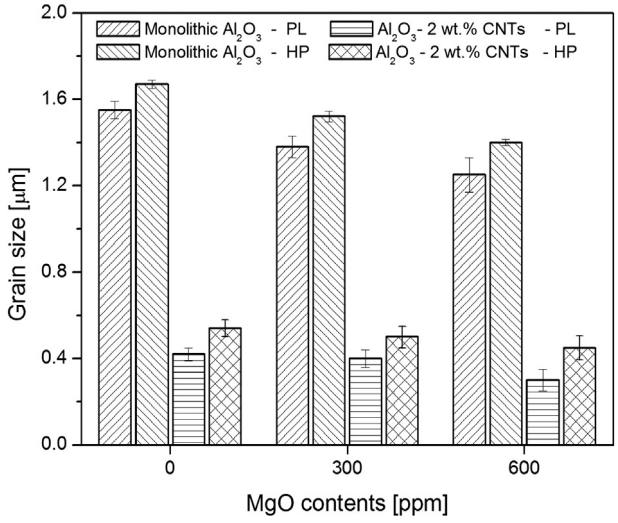

Fig. 5. Influence of the MgO contents on the grain size of the monolithic Al_2O_3 and nanocomposites consolidated by PL-sintering and HP-sintering.

Al_2O_3 grain boundaries to act as a pinning agent, because some studies showed that MWCNTs could be dispersed homogenous only up to very low levels (2 wt.%) [20]. Therefore, grain refinement in the tuned nanocomposites is probably due to the precipitates of magnesium-aluminate-spinel phase ($MgAl_2O_4$) that were present throughout the microstructure and formed thermodynamically from the MgO–Al_2O_3 system through phase transformation process [19]. The XRD pattern of the MgO-tuned Al_2O_3 (Fig. 7a) indicated the presence of diffraction peaks which are characteristics of the $MgAl_2O_4$ phase (JCPDS card no. 01-073-1959). Furthermore, the elemental constituents of the samples were confirmed from EDS analysis (Fig. 7c), spotted on areas marked by white arrows in the thermally etched micrograph (Fig. 7b) of the MgO-tuned sample. Presumably, these submicron sized precipitates effectively pinned the grains of the tuned nanocomposites to produce fine grain microstructures.

HP-sintered samples revealed exciting microstructural features as graphically represented in Fig. 7. Regardless of the MgO addition, pure Al_2O_3 and nanocomposites, exhibited slightly larger grain sizes than similar PL-sintered samples, respectively. The development of large grains with homogenous sizes during the pressure-assisted sintering, as shown in the SEM images of the fractured surface in Fig. 8, may be attributed to the reduced magnitude of drag forces on boundary motion. The applied pressures during sintering increased the consolidation rate, thus causing reduction of drag forces. The high sintering temperature, used to densify the samples, together with the presence of external pressure, could lead to unfavourable environment for grain growth, as suggested in an earlier study.

Furthermore, the microstructural features presented in Fig. 8 provide an in-depth insight into the role of the MgO in nanocomposites, because MgO-free nanocomposite samples presented numerous microscale structural flaws (white arrows in Fig. 8d) which are larger in dimensions and thicker in population. After MgO addition at either levels (300 or 600 ppm), an obvious change in the microstructures was observed as demonstrated in Fig. 8e and f, where a significant drop in the destiny of structural defects is evident. These findings support that MgO plays a significant role in altering the sintering mechanism, thereby leading to the production of far better and more homogenous microstructures in nanocomposites by somehow offsetting the apparent disadvantages due to the inclusion of MWCNTs. Therefore,

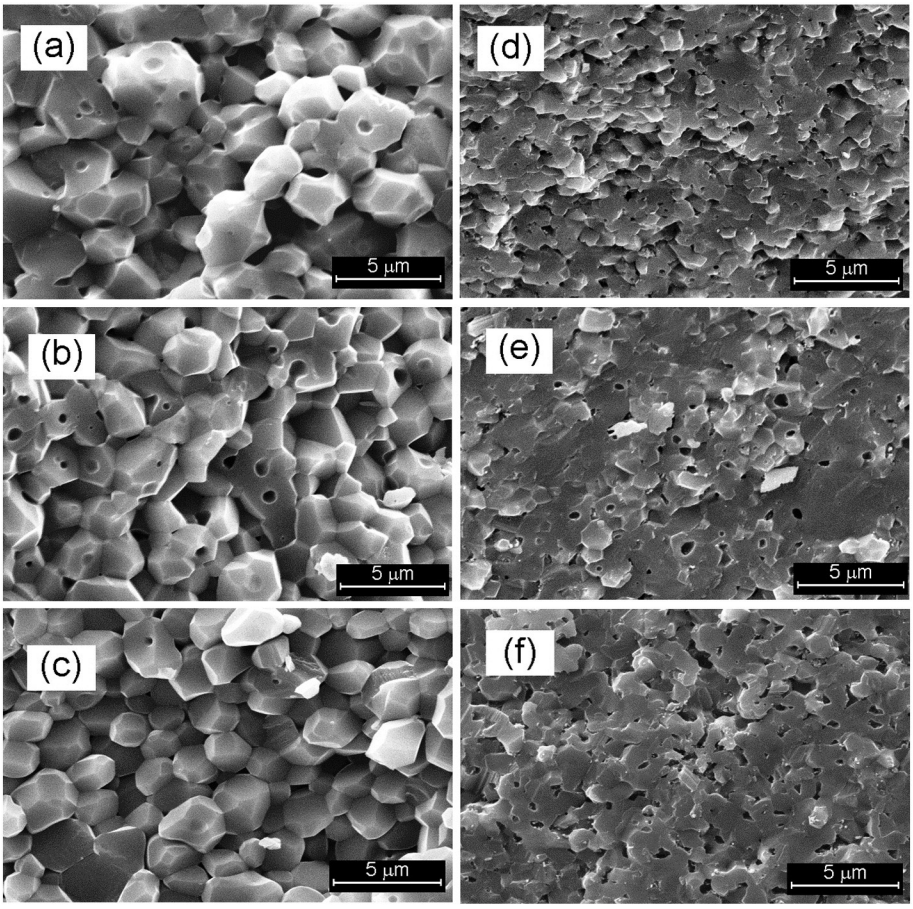

Fig. 6. Fractured surface SEM images of the samples that underwent PL-sintering, (a) untuned Al_2O_3, (b) 300 ppm MgO-tuned Al_2O_3, (c) 600 ppm MgO-tuned Al_2O_3, (d) untuned nanocomposite, (e) 300 ppm MgO-tuned nanocomposite and (f) 600 ppm MgO-tuned nanocomposite.

higher densities were obtained than those nanocomposites without MgO. Indeed, this MgO-tuned structural modification in nanocomposites is fairly advantageous in enhancing the degree of interaction between the MWCNTs and the Al_2O_3 matrix, allowing for MWCNTs to exhibit improved crack bridging and/or pull-out toughening capacities [4,5,11,14].

3.4. Mechanical properties

Hardness measurements showed a 5% drop in hardness in the nanocomposites (16.2 GPa) from that of monolithic Al_2O_3 (17.1 GPa) sintered under similar PL-sintering conditions without any MgO tuning. It is a fact that, even if homogenously dispersed as second phase, MWCNTs showed unfavourable effects on some important sintering mechanisms such as material diffusion and porosity elimination, thus resulting in nanocomposites with poor densification, weak MWCNT/matrix interface and reduced hardness [11,14]. Fig. 9 shows that as opposed to MgO-free samples, the PL-sintered monolithic Al_2O_3 (17.6 GPa) and nanocomposites (18.4 GPa) exhibited a higher hardness after tuning with 300 ppm MgO. Meanwhile, a further increase of the MgO content to 600 ppm did not appear to have any significant effect on hardness (18.5 GPa). The 12% increase in the hardness of the nanocomposites after 300 ppm MgO additions is possibly due to the lower sintering temperature during the PL-sintering which allows MWCNTs to attach firmly with the Al_2O_3 grains for performing strengthening mechanisms, as described in earlier studies [4,11]. Moreover, the higher hardness in the case of MgO-doped nanocomposites may also be associated with the appearance of fine-grained microstructures (Fig. 6). In ceramic nanocomposites, grain boundaries are potential pinning sites in the matrix microstructures, offering obstacles for dislocation to move across their respective microstructures by obstructing the onset of plasticity, thus a finer-grained microstructure as in cases of ceramic nanocomposites possesses increased the hardness value [20]. Fig. 9 further illustrates that the untuned and MgO tuned nanocomposites (300 and 600 ppm), upon HP-sintering treatment, show improvements in hardness by 15, 12 and 14%, respectively, when compared with their PL-sintered nanocomposite counterparts. On the basis of these hardness results, it can be deduced that the presence of external pressure during the high temperature sintering process is vital to increase the degree of interaction amongst the reinforcing MWCNTs and the Al_2O_3 matrix, which is highly desirable for good matrix/reinforcement cohesion [11,12]. Certainly, external pressure applied during the HP-sintering enhances the MWCNT/Al_2O_3 adhesion and improves consolidation through the elimination of microstructural defects; whilst at the same time, the MgO addition controls the sintering mechanisms thereby increasing their hardness in the doped-nanocomposites.

Accurate measurement of the K_{IC} in MWCNT–reinforced ceramics is challenging and the adopted indent crack length based techniques are unreliable due to inconsistent values [35]. For example, Sarkar and Das [28], calculated K_{IC} values of the Al_2O_3–MWCNT nanocomposites by employing DCM method using Niihara and Liang models and reported better K_{IC} values than those obtained using (single-edge notched beam) SENB technique whereas Ahmad et al. [14], reported higher K_{IC} values attained from SENB method than those obtained from the DCM method using the Chantikul model. These conflicting reports suggest that engineering components cannot be validated for structural load-bearing applications using DCM method; however, this convenient method is widely employed for K_{IC} comparisons [11]. In this regard, owing to prevailing doubts on its reliability, the DCM method employed

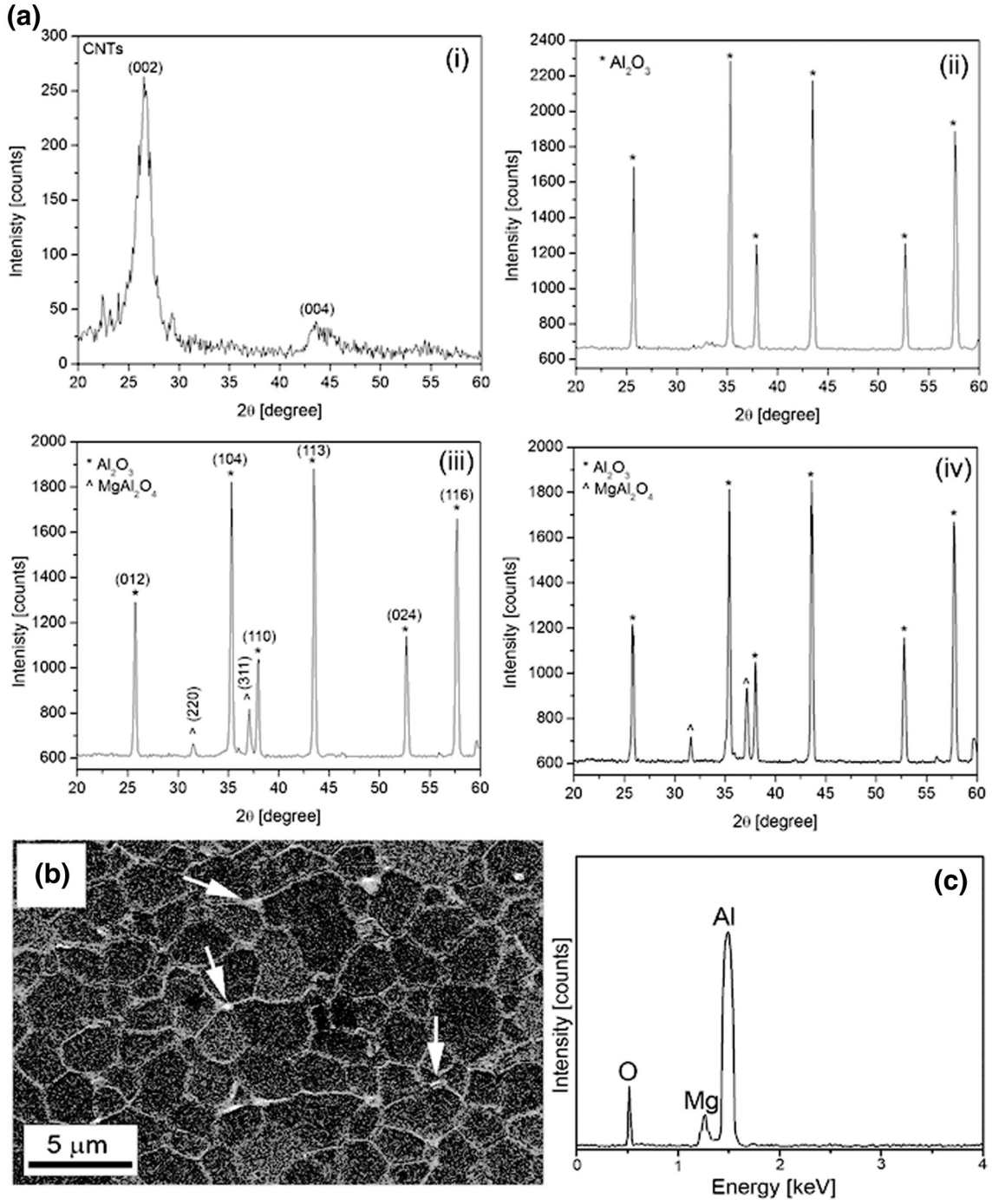

Fig. 7. (a) XRD patterns of (i) pristine MWCNT, (ii) monolithic Al_2O_3, (iii) 300 ppm MgO-tuned Al_2O_3, (iv) 600 ppm MgO-tuned nanocomposite, (b) SEM micrograph of thermally etched 600 ppm MgO-tuned Al_2O_3 showing precipitates of $MgAl_2O_4$ at Al_2O_3 grain boundaries (white arrows) and (c) chemical composition of the same precipitates confirming the elements of sample constituents.

in this study is used merely to provide reference K_{IC} values for comparing K_{IC} values of all the sintered samples.

In monolithic Al_2O_3 ceramic, the low K_{IC} and σ_f are usually attributed to structural inhomogeneities (flaws and porosity), deprived grain traits (weak grain bonding, large grain size) and brittle failure mechanism (intergranular fracture mode) [20]. HP-sintered monolithic Al_2O_3 samples with or without MgO, produced during this work, demonstrated almost similar results (Table 1) which are in good agreement with previous reports [4,5,11]. After MWCNT's incorporation, the resulting MgO-free nanocomposites showed reasonable increases in the K_{IC} (22%) and σ_f (12%) values against the monolithic Al_2O_3 (Table 1). Earlier studies suggested that the unique nanoscale features and firm interface facilitate MWCNTs to perform efficient load-sharing between the MWCNT and the Al_2O_3 matrix through proposed matrix grain sharing and crack bridging toughening mechanisms for higher K_{IC} and σ_f [5,8,13]. Furthermore, strengthening of Al_2O_3 boundaries by MWCNTs is also evident from the appearance of the transgranular fracture mode in the nanocomposites (Fig. 8b) rather than the typical intergranular fracture mode which usually occurs in the monolithic Al_2O_3 (Fig. 8a). The fractured surface details provide strong evidence about MWCNT's contribution towards strengthening the Al_2O_3 matrix grains, because the transgranular fracture dominates only when the strength of the grain boundary is close to that of the matrix grain [37]. It means that the firmly bonded MWCNTs surely supported the Al_2O_3 matrix to

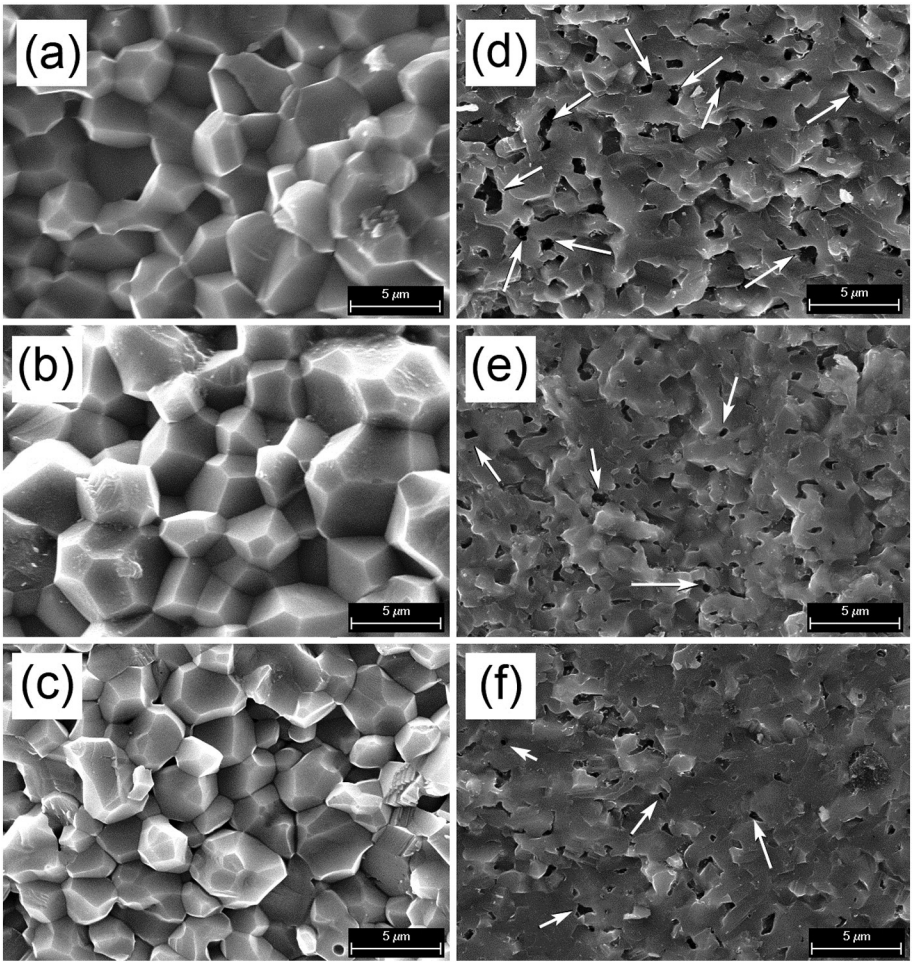

Fig. 8. Fractured surface SEM images of the HP-sintered monolithic Al_2O_3 tuned with MgO contents (a) 0 ppm, (b) 300 ppm and (c) 600 ppm and nanocomposites tuned with MgO (d) 0 ppm, (e) 300 ppm and (f) 600 ppm contents.

transfer fracture through the grains rather than along grain boundaries, as is the case with monolithic Al_2O_3.

Compared with the MgO-free nanocomposite samples, reasonable rises in the values of K_{IC} (by 15 and 20%) and σ_f (by 5 and 10%) were gained upon MgO additions by as small amounts as 300 and 600 ppm.

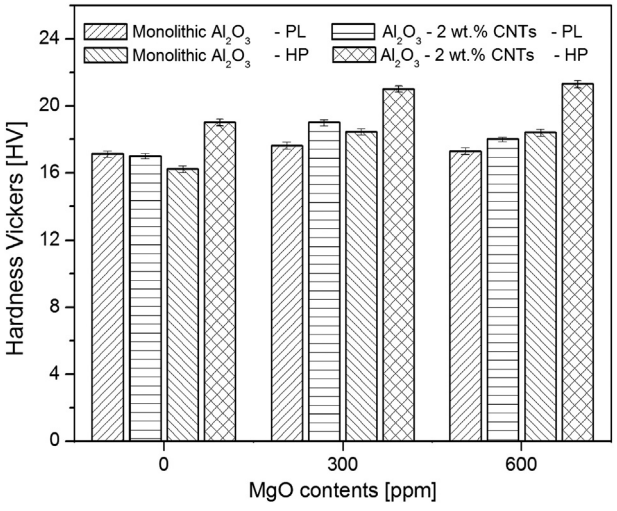

Fig. 9. Hardness Vickers profile of the monolithic Al_2O_3 and nanocomposites tuned with various (300 and 600 ppm) MgO contents and sintered with and without external pressures.

Nanocomposites tuned with 600 ppm MgO demonstrated best K_{IC} and σ_f values of 5.1 MPa·m$^{1/2}$ and 435 MPa, respectively, which are 37 and 22% higher than those for the monolithic Al_2O_3 *i.e.* K_{IC} = 3.2 MPa·m$^{1/2}$ and σ_f = 340 MPa, fabricated under identical processing conditions. Apparently transgranular fracture mode was noted in the nanocomposite samples tuned with either MgO levels (Fig. 8e and f). Although a superior mechanical response of ceramic composites is generally attributed to the fine-grained microstructure however, the existence of elongated pores in our MgO-free nanocomposite fractograph (white arrows in Fig. 8d) had certainly curtailed the benefit of grain refinement, thus leading to deprive K_{IC} and σ_f, as shown in Table 1. This implies that whilst MgO tuning barely affected the fracture behaviour of the nanocomposites, it contributed to the improved mechanical properties, probably by means of microstructural modification.

Analysis of the MgO-doped nanocomposite fractographs facilitated an in-depth understanding of the role of MgO in improving the K_{IC} and σ_f. Numerous structural flaws are obvious in the MgO-free nanocomposite fractograph (Fig. 8d), however flaw reductions were observed in the MgO-tuned nanocomposites (Fig. 8e and f). In ceramic nanocomposites, microstructural flaws are a potential reason for low fracture resistance because the fracture strength (σ_F) depends on the flaw (c), according to an empirical square-root relationship $\sigma_F \propto l^{-0.5}$, where the value of c is calculated using grain size (l) [19,38]. Further, higher residual defect (pores/flaws) densities will lower the stress required for the crack initiation. Similar defects were observed in the MgO-free nanocomposite fractograph (see Fig. 8d). Based on the information from fractured surfaces, it may be deduced that failure in the neat nanocomposites might have been initiated around these flaws in

terms of stress concentration. Since the MgO addition improved the nanocomposite densities by lowering sintering temperatures and segregation of the $MgAl_2O_4$ phase, preferably at Al_2O_3 grain junctions in the tuned nanocomposites, two potential benefits are the elimination of residual flaws and grain refinement. The apparent drop in structural defect density certainly minimizes the number of stress concentration sites together with fine-grained structure that is beneficial to the increased critical strain-energy release rate which provides more crack deflections during the course of failure. The net contribution is superior mechanical properties of the nanocomposites than pure Al_2O_3 in terms of increases in toughness, flexibility and hardness by 37, 22 and 20%, respectively. We also compare our K_{IC} and σ_f results with values extracted from the previous studies on Al_2O_3 nanocomposites containing ~2 wt.% MWCNTs and an obvious difference was noted, as graphically presented in Fig. 10 [12,28,31,33–36,39,40]. It seems that the enhancements in mechanical properties (K_{IC}, σ_f) recorded in our case are presumably due to the cumulative effect of the uniform MWCNT dispersion and the MgO incorporation. The MgO incorporation altered the sintering characteristics of nanocomposites by curtailing the densification hurdle generated by MWCNTs, also by tuning the microstructures of the matrix with fine grains and few defects.

4. Conclusions

The effects of MgO addition on microstructure and mechanical properties, at 300 and 600 ppm loading levels for 2 wt.% MWCNT–reinforced Al_2O_3 nanocomposites sintered by PL and HP techniques, were systematically investigated. The uniform MWCNT dispersion within the Al_2O_3 matrix was successfully achieved through optimization of surfactant-assisted and wet chemistry route. PL-sintering with and without any MgO addition could not consolidate nanocomposites to well-integrated microstructures with marginal differences in densities and hardness values when compared with MgO-free nanocomposite samples. HP-sintering and MgO addition had combined effects on the reduction in the residual pores/flaw density and dimensions through modification of the sintering mechanism, thus consolidating the nanocomposites to near-theoretical densities (~99.6%) with well-integrated microstructures. HP-sintered nanocomposites tuned with MgO (0, 300 and 600 ppm) demonstrated higher hardness levels by 15, 12 and 14%, respectively, when compared with their PL-sintered nanocomposite counterparts. Moreover, MgO additions led to further improvement on hardness (10 and 11%), flexural strength (5 and 10%) and fracture toughness (15 and 20%). Finally, an overall enhancement of 37, 22 and 20% in fracture toughness, flexural strength and hardness respectively, was obtained in the HPed nanocomposites containing 600 ppm MgO, against the monolithic Al_2O_3.

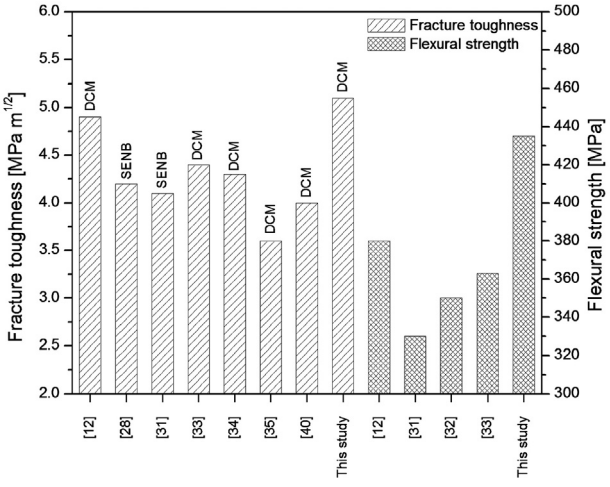

Fig. 10. Comparison of the (a) K_{IC} and (b) σ_f values obtained in the present study with previous reports.

Acknowledgements

The authors gratefully acknowledge the technical and financial support of Research Center of College of Engineering, Deanship of Scientific Research, King Saud University, Riyadh, Kingdom of Saudi Arabia.

References

[1] G.E. Gadd, M. Blackford, S. Moricca, N. Webb, P.J. Evans, A.M. Smith, Q. Hua, The world's smallest gas cylinders, Science 277 (1997) 933–936.
[2] M.F. Yu, O. Lourie, M.J. Dyer, K. Moloni, T.F. Kelly, R.S. Ruoff, Science 287 (2000) 637.
[3] H. Ohnabe, S. Masaki, T. Sasa, Potential application of ceramics matrix composites to aero-engine components, Composites A 30 (1999) 489–496.
[4] E. Zapata-Solvas, D. Gómez-García, A. Domínguez-Rodríguez, Towards physical properties tailoring of carbon nanotubes–reinforced ceramic matrix composites, J. Eur. Ceram. Soc. 32 (2012) 3001–3020.
[5] J. Cho, A.R. Boccaccini, M.S.P. Shaffer, Ceramic matrix composites containing carbon nanotubes, J. Mater. Sci. 44 (2009) 1934–1951.
[6] A. Kasperski, A. Weibel, C. Estourne's, C. Laurent, A. Peigney, Multi-walled carbon nanotube–Al_2O_3 composites: covalent or non-covalent functionalization for mechanical reinforcement, Scr. Mater. 75 (2014) 46–49.
[7] A. Kasperski, A. Weibel, C. Estourne's, C. Laurent, A. Peigney, Preparation microstructure–property relationships in double-walled carbon nanotubes/alumina composites, Carbon 53 (2013) 62–72.
[8] H. Ondrej, S. Jaroslav, S. Pavol, New approach for distribution of carbon nanotubes in alumina matrix, J. Eur. Ceram. Soc. 34 (2014) 1845–1851.
[9] E. Flahaut, A. Peigney, C. Laurent, C. Marlière, F. Chastel, A. Rousset, Carbon nanotube–metal–oxide nanocomposites: microstructure, electrical conductivity and mechanical properties, Acta Mater. 48 (2000) 3803–3812.
[10] M. Estili, A. Kawasaki, H. Sakamoto, Y. Mekuchi, M. Kuno, T. Tsukada, The homogeneous dispersion of surfactantless, slightly disordered, crystalline, multiwalled carbon nanotubes in α-alumina ceramics for structural reinforcement, Acta Mater. 56 (2008) 4070–4079.
[11] S. Sarkar, P.K. Das, Processing and properties of carbon nanotube/alumina nanocomposites: a review, Rev. Adv. Mater. Sci. 37 (2014) 53–82.
[12] I. Ahmad, A. Kennedy, Y.Q. Zhu, Multi-walled carbon nanotubes reinforced Al_2O_3 nanocomposites: mechanical properties and interfacial investigations, Compos. Sci. Technol. 70 (2010) 1199–1206.
[13] F. Inam, T. Pijis, M.J. Reece, The production of advanced fine-grained Al_2O_3 by carbon nanotubes addition, J. Eur. Ceram. Soc. 31 (2011) 2853–2859.
[14] I. Ahmad, H. Cao, H. Chen, H. Zhao, A. Kennedy, Y.Q. Zhu, Carbon nanotube toughened aluminium oxide nanocomposites, J. Eur. Ceram. Soc. 30 (2009) 865–873.
[15] Y.K. Jeong, A. Nakahira, K. Niihara, Effects of additives on microstructure and properties of Al_2O_3–silicon carbide nanocomposites, J. Am. Ceram. Soc. 82 (1999) 3609–3612.
[16] I. Ahmad, M.A. Dar, Structure and properties of Y_2O_3-doped Al_2O_3–MWCNT nanocomposites prepared by PL-sintering and hot-pressing, J. Mater. Eng. Perform. 23 (2014) 2110–2119.
[17] D.A. Rani, Y. Yoshizawa, K. Hirao, Y. Yamushi, Effect of rare-earth dopants on mechanical properties of Al_2O_3, J. Am. Ceram. Soc. 87 (2004) 289.
[18] S. Lartigue, C. Carry, L. Priester, Grain boundaries in high temperature deformation of yttria and magnesia Co-doped Al_2O_3, J. Phys. Colloq. 51 (1990) 985–990.
[19] K. Kosmac, S. Wallance, N. Claussen, Influence of MgO addition on the microstructure and mechanical properties of Al_2O_3–ZrO_2 composite, Comm. Am. Ceram. Soc. (1982) 66–67.
[20] I. Ahmad, M. Islam, A.A. Almajid, B. Yazdani, Y.Q. Zhu, Investigation of yttria-doped Al_2O_3 nanocomposites reinforced by multi-walled carbon nanotubes, Ceram. Int. 40 (2014) 9327–9335.
[21] A. Rittidech, L. Portia, T. Bongkarn, The relationship between microstructure and mechanical properties of Al_2O_3–MgO ceramics, Mater. Sci. Eng. (2006) 395–398.
[22] C.P.S. Kumar, B. Baron, S. Hampshire, Effect of dopants on densification, microstructure and mechanical properties of alumina–silicon nanocomposites ceramics prepared by pressureless sintering, J. Eur. Ceram. Soc. 24 (2004) 3317–3326.
[23] C. Laurent, E. Flahaut, A. Peigney, The weight and density of carbon nanotubes versus the number of walls and diameter, Carbon 48 (2010) 2989–2999.
[24] B.D. Cullity, S.R. Stock, Elements of X-ray Diffraction, 3rd ed. Prentice-Hall, Inc., New Jersey, 2009. 93 (ISBN: 0-13-178818-3).
[25] F. Inam, H. Yan, M.J. Reece, T. Peijs, Structural and chemical stability of multiwall carbon nanotubes in sintered ceramic nanocomposite, Adv. Appl. Ceram. 109 (2010) 240–247.
[26] K.M. Liew, C.H. Wong, X.Q. He, M.J. Tan, Thermal stability of single and multi-walled carbon nanotubes, Phys. Rev. B71 (2005) 075424.
[27] D. Chakravarty, R. Sundaresan, Spark plasma sintering of magnesia-doped alumina with high hardness and fracture toughness, J. Am. Ceram. Soc. 91 (2008) 203–208.
[28] S. Sarkar, P.K. Das, Microstructure and physico-mechanical properties of pressureless sintered multi-walled carbon nanotubes/alumina nanocomposites, Ceram. Int. 38 (2012) 423–432.
[29] K. Satoshi, T. Matsudaira, W. Masashi, Mass-transfer mechanism of alumina ceramics under oxygen potential gradients at high temperatures, Mater. Trans. 50 (2009) 1023–1031.

[30] F. Jianxin, A.M. Thompson, M.P. Harmer, H.M. Chan, Effect of yttrium and lanthanum on the final-stage sintering behavior of ultrahigh-purity Al_2O_3, J. Am. Ceram. Soc. 80 (1997) 2005–2012.
[31] T. Wie, Z. Fan, F. Wie, A new structure for multi-walled carbon nanotubes reinforced alumina nanocomposite with high strength and toughness, Mater. Lett. 62 (2008) 641–644.
[32] G. Yamamoto, M. Omori, T. Hashida, H. Kimura, A novel structure for carbon nanotube reinforced alumina composites with improved mechanical properties, Nanotechnology 19 (2008) 315708.
[33] H. Ghobadi, N. Ali, T. Ebadzade, Z. Sadeghian, H. Barzegar-Bafrooei, Improving CNT distribution and mechanical properties of MWCNT reinforced alumina matrix, Mater. Sci. Eng. A 617 (2014) 110–114.
[34] N. Ueda, T. Yamakami, T. Yamaguchi, S. Taruta, Influence of CNF content on microstructure and fracture toughness of CNF/alumina composites, J. Ceram. Soc. Jpn. 122 (2014) 292–299.
[35] N. Bakhsh, F.A. Khalid, A.S. Hakeem, Effect of sintering temperature on densification and mechanical properties of pressureless sintered CNT–alumina nanocomposites, Mater. Sci. Eng. 60 (2014) 012059.
[36] Z.Y. Deng, T. Ohiji, Fracture-mode change in alumina–silicon carbide composites tuned with rare-earth impurities, J. Am. Ceram. Soc. 86 (2003) 1789–1792.
[37] B.W. Sheldon, W.A. Curtin, Nanoceramic composites: tough to test, Nat. Mater. 3 (2004) 505–506.
[38] B.N. Kim, S. Wakayama, M. Kawahara, Characterization of 2-dimensional crack propagation behaviour simulation and analysis, Int. J. Fract. 75 (1996) 247–259.
[39] P. Chantikul, S.J. Bennison, B.R. Lawn, Role of grain size in the strength and R-curve performance of alumina, J. Am. Ceram. Soc. 73 (1990) 2419.
[40] C.N. He, F. Tian, S.J. Liu, A carbon nanotube/alumina network structure for fabricating alumina matrix composites, J. Alloys Compd. 478 (2009) 816–819.